Journal of Materials Processing Technology 210 (2010) 1260–1269

Contents lists available at ScienceDirect

Journal of Materials Processing Technology

journal homepage: www.elsevier.com/locate/jmatprotec

An experimental and computational methodology for near net shape fabrication of thin walled ceramic structures by plasma spray forming

Riken R. Patel [a], Anup Kumar Keshri [a], George S. Dulikravich [b], Arvind Agarwal [a,*]

[a] Plasma Forming Laboratory, Department of Mechanical and Materials Engineering, Florida International University, 10555 West Flagler Street, EC 3464, Miami, FL 33174, United States

[b] Multidisciplinary Analysis, Inverse Design, Robust Optimization and Control Laboratory, Department of Mechanical and Materials Engineering, Florida International University, 10555 West Flagler Street, EC 3464, Miami, FL 33174, United States

ARTICLE INFO

Article history:
Received 27 October 2009
Received in revised form 15 January 2010
Accepted 13 March 2010

PACS:
44.05.+e
44.10.+I
44.15.+a
44.25.+f
44.27.+g
44.35.+c
45.10.−b
47.11.Df
47.11.Fg
52.77.Fv
81.05.Je

Keywords:
Near net shape
Plasma spray forming
Ceramic
Aluminum oxide
Computation
Algorithm

ABSTRACT

Near net shape (NNS) fabrication by plasma spray forming (PSF) is a rapid prototyping technique to fabricate engineering components having axi-symmetric geometry out of ceramics and refractory metals which are difficult to manufacture by conventional techniques. This study establishes an experimental and computational protocol to manufacture thin walled ceramic (Al_2O_3) structures on the graphite mandrel (substrate) via plasma spray forming. The combination of experimental and computational approaches reduces currently used empirical methods for the similar purpose. Thermal profiles generated during plasma spraying of Al_2O_3 on the graphite mandrel for various mandrel designs and cooling conditions were computed by solving the conjugate problem of computational fluid dynamics and 3D unsteady heat transfer. Entire plasma spraying booth was modeled as per actual dimensions to consider the effect on the thermal profile of the mandrel/coating system. The computed temperature profile was compared with the experimentally measured temperature. The corresponding thermal stresses in the mandrel and spray deposited Al_2O_3 layer were computed. Computed thermal stresses were compared with the fracture strength of Al_2O_3 to prevent cracking of the spray formed structure during spraying and its successful removal from the mandrel. An optimum temperature increase rate (TIR) during plasma spray forming is defined for the successful deposition and removal of the freestanding ceramic structure.

1. Introduction

Near net shape (NNS) forming by plasma spray technique is a rapid manufacturing process that provides feasibility of fabricating axi-symmetric, free standing, thin walled (~1 mm) contoured structures from ceramics, metal matrix composites, intermetallics and refractory metals which are difficult to manufacture by conventional techniques like casting, forging or powder metallurgy (Agarwal et al., 2002; Fang and Xu, 2002). Researchers have demonstrated the feasibility of fabricating free-standing components using several combinations of mandrels/substrates and coatings in the following studies. Agarwal et al. (2002) synthesized nanostructured Al_2O_3 free standing cylindrical structures of thickness 0.4–0.6 mm on 6061 aluminum mandrel by PSF. Complex geometries like nozzles, cones and cylinders of thickness up to 3 mm of nickel and yttria–8 wt.% zirconia (Devasenapathi et al., 2002) and free standing annular ring structure of 20 mm diameter, 8 mm width and 3 mm thickness of Al_2O_3–40 wt.% TiO_2 composite (Gopalakrishnan et al., 2003) were also fabricated. Radially symmetric, free-standing yttria stabilized zirconia conical structures of 1.2 mm thickness (Fogarassy et al., 2004) and thin walled tungsten (W) nozzle liner and non-eroding rhenium (Re) throat on reusable graphite mandrel (Balani et al., 2006) were manufactured using PSF technique. Free standing HfC rings of 12 mm diameter (Agarwal et al., 2001), thin walled zero erosion refractory metal/ceramic nozzles inserts for solid rocket propulsion (Hickman et al., 2001)

* Corresponding author. Tel.: +1 305 348 1701; fax: +1 305 348 1932.
E-mail address: agarwala@fiu.edu (A. Agarwal).

0924-0136/$ – see front matter © 2010 Elsevier B.V. All rights reserved.
doi:10.1016/j.jmatprotec.2010.03.012

and lightweight space based X-ray optics (Agarwal and McKechnie, 2001) have also been formed by plasma spray forming.

Most of the above-listed studies were done empirically using a trial and error approach. There is no well established engineering protocol or algorithm described to develop free-standing components by customizing the plasma parameters, spray material and mandrel material for near net shape forming. Hence this study was aimed to develop an algorithm to predict the result of the near net shape manufacturing process via PSF. This algorithm can be applied to predict the removability of intact free-standing component for a given combination of coating and mandrel material. It is envisaged that this computational and experimental based manufacturing protocol will minimize trial and error method and can be applied to manufacture engineering components for a variety of ceramic coatings and mandrels with minor modifications.

2. Formulation of the problem

Plasma spraying involves significant amount of heat transfer during coating deposition and post-spray cooling. The rapid temperature change of the mandrel and spray deposit creates residual stresses in the mandrel/coating system. Excessive heating or cooling rate could lead to thermal shock and induce cracking in thin walled ceramic coating. The current state of the art for near net shape formation by PSF is limited to empirical approach and do not utilize an engineering protocol to account for thermal effects in forming and removability of the spray deposited structure. Hence in the present study the computational and experimental algorithm has been developed that takes in to consideration the effect of *mandrel design* and *heat transfer* on the removability of near net shape structure by following the flow diagram illustrated in Fig. 1.

The present study adopts a non-destructive technique to separate spray deposited ceramic structure from the mandrel by utilizing the difference in coefficient of thermal expansion (CTE) of the mandrel and the spray deposited material. The successful removal of the spray formed component also depends on the overall residual stresses induced in the process. The overall residual stress in ceramic coating is defined as the summation of thermal stress (generated due to temperature mismatch) and quenching stress (25–50 MPa for ceramics) (Kuroda and Clyne, 1991). Thermal stress can be controlled by degree of heating and cooling. Hence thermal analysis was carried out for the selected mandrel material and geometry, coating, cooling conditions and plasma parameters. Thermal profile generated during plasma spraying and post-spray cooling in the mandrel/coating system was computed by solving the combined computational fluid dynamics and 3D unsteady heat transfer with the aid of ANSYS workbench 11.0–CFX^{TM}. Computed thermal profile in the mandrel was compared and validated by experimentally measuring temperature distribution by placing thermocouples at strategic locations in the mandrel. Thus validated temperature profile of mandrel was mapped in to ANSYS^{TM} simulation and structural module by one-way coupling to determine corresponding thermal stresses in the mandrel and spray deposited coating. The overall residual stress developed in the sprayed formed component was calculated based on the computed thermal stress and quenching stress of 25–50 MPa. The overall residual stresses

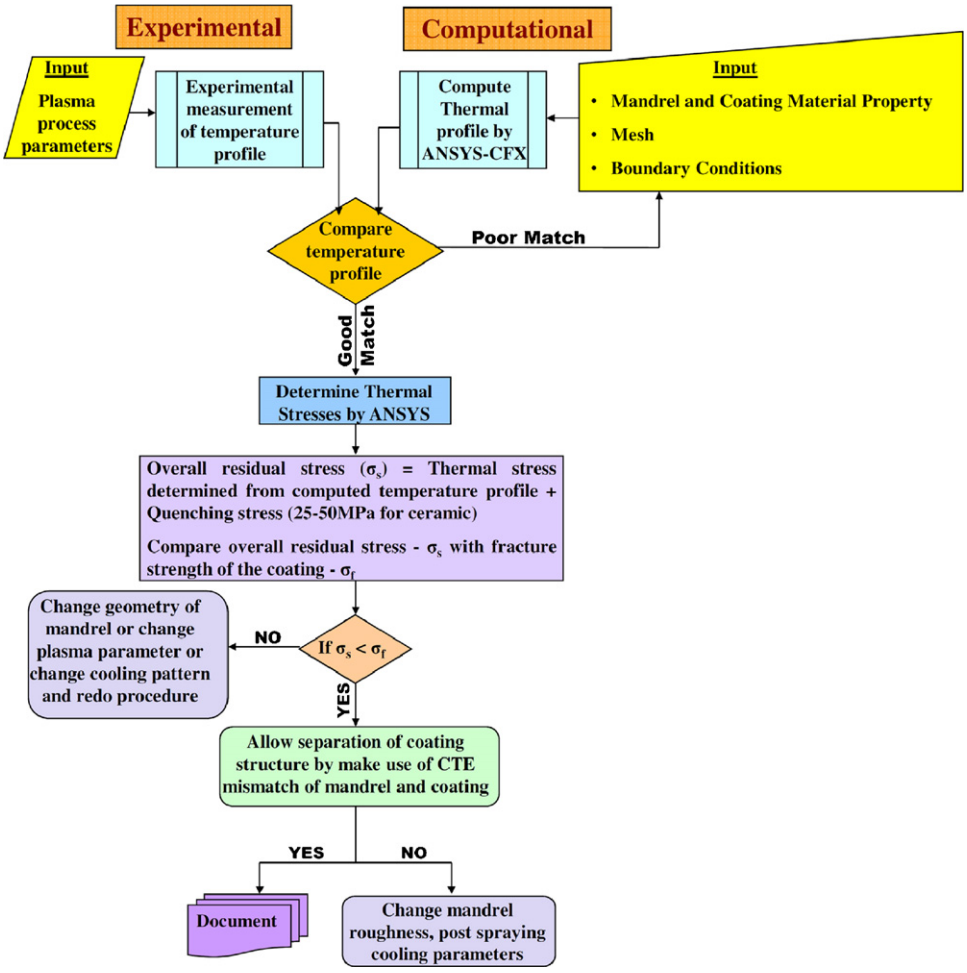

Fig. 1. Overall research approach for the experimental and computational work.

were compared with the fracture strength of the coating to predict prevention of cracking and its removability from the mandrel. The results were verified by carrying out experiments for selected mandrel/coating system and cooling conditions.

3. Experimental work

One of the specific objectives to achieve overall goal was to measure the temperature profile of the mandrel/coating system for varying mandrel designs in the presence of different cooling media during fabrication of a thin walled ceramic structure by plasma spraying. The experimental procedure to conduct these studies is described herewith.

3.1. Coating material

Al_2O_3 powder (99.0% pure, −45 μm/+5 μm particle size) obtained from Praxair Surface Technologies (Danbury, CT, USA) was used as the feedstock material for ceramic coating deposition on the mandrel

3.2. Mandrel material

An ideal mandrel material for plasma spray forming (PSF) should possess ease of machinability, withstand heat during plasma spraying and not chemically react with the spray deposited material. The mandrel should be easily removable after the desired material has been sprayed. The goal of this study is to separate spray deposited Al_2O_3 structure from the mandrel by utilizing the difference in coefficient of thermal expansion (CTE) of the mandrel and coating. The separation of the spray deposited structure from the mandrel depends on several variables like heating and cooling rates and maximum temperature attained by the mandrel during and after plasma spraying. Rapid increase of the temperature may generate cracks in the coating as thermal expansion rate of mandrel (metallic or non-metallic) and ceramic coating are different. Also, mandrel temperature should be maintained significantly below its softening/melting point to avoid damage. Based on these criteria, Graphite (POCO EDM II) was used as the mandrel material for this study. Graphite has a coefficient of thermal expansion of 8.0×10^{-6} °C (Gauthier, 1995) which is slightly higher than CTE of Al_2O_3 7.6×10^{-6} °C (McColm, 1994). A similar but slightly higher CTE for the mandrel would result in its greater shrinkage during post-spray cooling and assist the release of thin ceramic coating. A higher difference between CTE of mandrel and coating is not desired as it is likely to increase the crack formation during plasma spraying. Mandrel surface finish is another important parameter that affects the coating deposition and its removability. A very smooth surface (R_a = few nm) will cause poor adherence of the coating to the mandrel whereas a very rough surface (R_a = several tens of microns) would create strong mechanical interlocking and hence coating separation will be difficult. In this study, graphite mandrel surface roughness was maintained uniform ($R_a \sim 1$ μm) for all experiments. This value was selected based on the previous experience (Agarwal et al., 2002).

3.3. Mandrel design

Mandrel design is a key parameter to determine heat transfer during and after spraying. Mandrel design evolution was a continual process during the course of this study. Improvements in the mandrel design were carried out based on the preliminary *experimental* and *computational* results of the temperature distribution.

Design modifications were made to enhance the heat transfer during and after spraying for effective mandrel temperature control. Generation-1 mandrel is a solid cylinder 38.1 mm $D \times 40$ mm L with four holes of 1.59 mm diameter at strategic locations for inserting thermocouples to measure the temperature during plasma spraying as shown in Fig. 2. The major drawback of the generation-1 mandrel design was the poor heat dissipation due to its solid geometry. This caused damage to the mandrel surface due to localized melting and/or softening due to high temperature during plasma spraying. The straight cylindrical edges of the mandrel would also pose difficulty in separation of the spray deposited coating. Generation-2 mandrel was similar to generation 1 design except with a gentle taper of 2° along the length. It was envisaged that gentle taper would ease the removal of spray deposited ceramic coating from the mandrel. However, generation-2 mandrel also suffered with poor heat dissipation due to its solid geometry. To overcome this limitation, Generation-3 mandrel (33.06 mm (D_1: bottom outer diameter) × 30.50 mm (D_2: top outer diameter) × 19.50 mm (D_3: inner diameter) × 40 mm L with a 2° taper along the length on the outer surface was designed to improve heat dissipation by making it hollow and creating six equiangular annular holes of 3 mm diameter as shown in Fig. 2. The major benefit of the hollow mandrel was an access to cool inner walls by supplying cooling media from the top. The bottom part of generation-3 mandrel was also hollow that snug fits on to a hollow shaft during spraying process and hence allows the cooling stream to pass through the mandrel assembly and bottom of the hollow shaft (Fig. 3). Generation-3 mandrel had a surface roughness (R_a) of

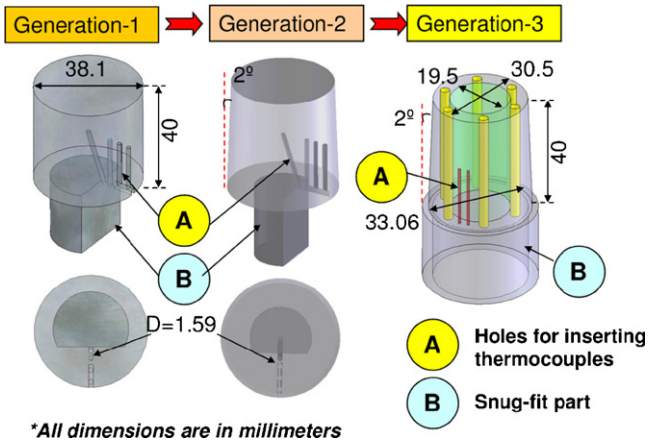

Fig. 2. Three generations of the mandrels.

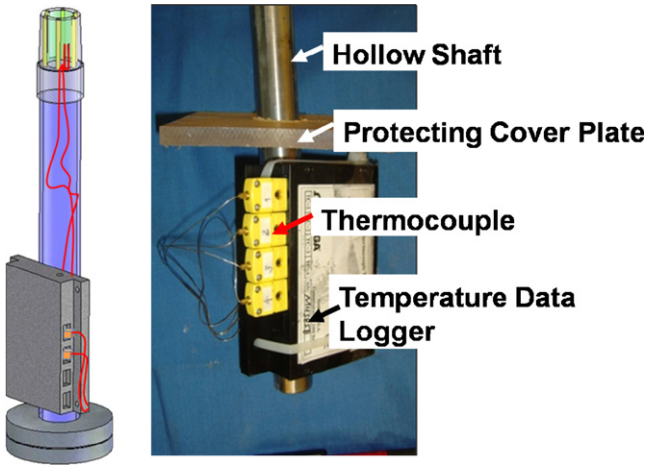

Fig. 3. Arrangement showing connection between thermocouples, mandrel and datalogger.

0.67 ± 0.10 μm. Surface roughness was maintained constant for all experiments.

3.4. Temperature measurement

The mandrel temperature was measured by two different approaches. The real time mandrel temperature variation during and after plasma spraying was measured by quick response thermocouples KMQSS-020U (Omega Engineering Inc.) inserted at the strategic locations as shown in Figs. 2 and 3. Data logger was mounted at the bottom of the hollow shaft (Fig. 3) to maintain physical connectivity with thermocouples (TC). The real time surface temperature of the mandrel during preheating and coating during deposition was measured by ultra high frequency (30 Hz) Raytek Raynger MX® infrared (IR) pyrometer which was placed at an angle of 45° at the back side of mandrel (Fig. 4(a)).

3.5. Plasma spraying

Plasma spraying facility at Plasma Forming Laboratory (PFL) at Florida International University was utilized for carrying out experiments for this study. A schematic of the experimental setup and photograph is shown in Fig. 4(a) and (b) respectively. Plasma spraying was carried by SG 100® plasma gun (Praxair Surface Technologies, Indianapolis, IN), with internal powder feeding. Plasma processing parameters utilized for the fabrication of near net shape Al_2O_3 are listed in Table 1.

The overall sequence and type of experiments were carried out based on the computational predictions and preliminary experimental results. Three to four experimental runs for each cooling condition and mandrel design were performed for consistency and repeatability check point of view.

4. Computational work

Mandrel *temperature* and subsequent *thermal stress* generated during process are the critical variables that govern successful deposition and removal of the near net shape ceramic structure. Hence in order to predict the temperature profile of the mandrel, the complex phenomenon involving conjugate problem of CFD and

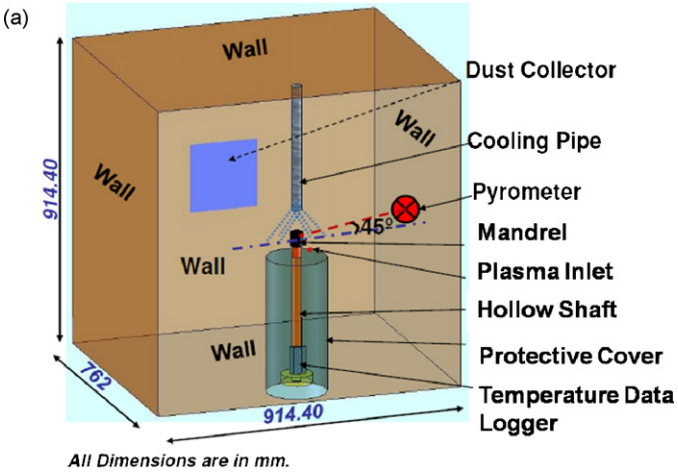

Fig. 4. (a) Schematic of plasma spray forming process inside the spray booth. (b) Actual experimental setup.

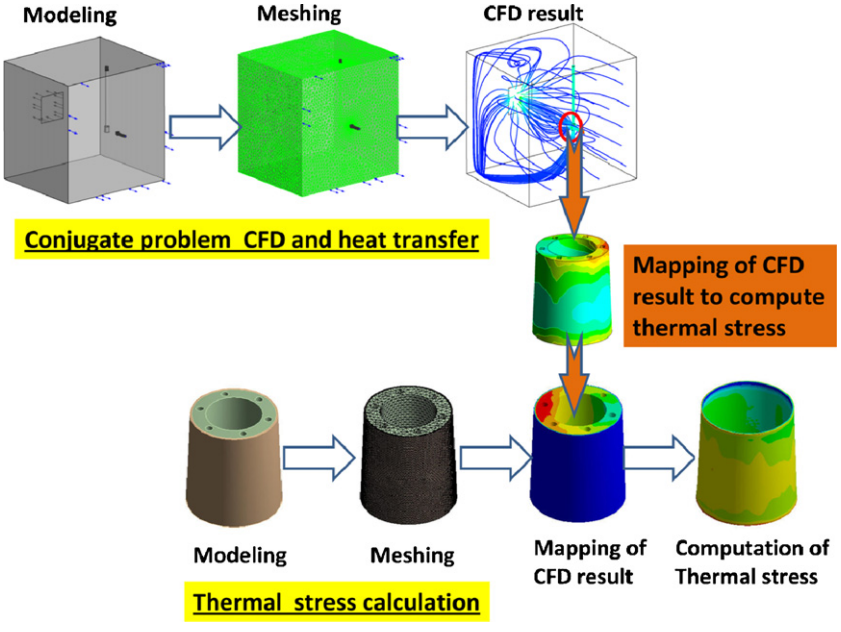

Fig. 5. One-way coupling of CFD and thermal stress analysis.

Table 1
Plasma process variables utilized for near net shape experiments.

Plasma process variables	Description
Plasma power (kW)	32
Powder feed rate (gm/min)	7.75
Primary, Ar (slm)	32.1
Secondary, He (slm)	59.5
Carrier, Ar (slm)	19.8
Standoff distance (mm)	100
Cooling media: (i) Air, (ii) liquid N_2, and (iii) Air + liquid N_2	
Pressure	1.2 bars
Location	50 mm from top of the mandrel

slm = standard liters per minute.

heat transfer was solved by modeling the entire plasma spraying booth at Plasma Forming Laboratory (PFL) at FIU as per the actual dimensions shown in Fig. 4 (a) and (b). Following approach was adopted to solve this complex problem as illustrated in Fig. 5.

i. Temperature profile of the mandrel during entire process was computed by solving conjugate problem of CFD and heat transfer by ANSYS CFX™ module that utilized finite volume method.
ii. Relative temperature distribution in the coating and mandrel was computed using finite element method. Temperature profile of the mandrel obtained from CFD analysis and experimentally measured coating temperature using IR pyrometer were used as input to solve the state steady state problem as depicted in Fig. 5.
iii. Relative temperature distribution was used to calculate thermal stress in coating. Temperature profile was computed considering all important physical conditions in form of boundary conditions and by solving complex problem of CFD and heat transfer.

4.1. Assumptions

Following assumptions were made for the computations.

- All walls of the plasma spray booth and cooling pipe were considered adiabatic.
- Based on the preliminary computations, it was found that the effect of the hollow shaft and protective cover for temperature data logger (Fig. 4(a)) on the mandrel temperature profile was negligible. Hence hollow shaft and protective cover were excluded from the subsequent calculations.
- The bottom of the mandrel bottom was considered stationary while computing thermal stress in the coating and mandrel.

4.2. Computational theory

ANSYS CFX™-11.0 solver was utilized to compute and solve complex conjugate phenomena that involved different fluid–fluid and fluid–solid interaction by finite volume method. CFD problem was solved by using well-known Navier–Stokes equations. The steady state problem was solved by utilizing following basic heat transfer equation that determined relative thermal profile in the mandrel and the coating.

$$\rho c\left(\frac{\partial T}{\partial t} + \{v\}^T \cdot \nabla T\right) = \nabla^T \cdot ([K]\nabla T) \quad (1)$$

where thermal conductivity matrix is $K = \begin{bmatrix} K_{xx} & 0 & 0 \\ 0 & K_{yy} & 0 \\ 0 & 0 & K_{zz} \end{bmatrix}$. Here K_{xx}, K_{yy}, K_{zz} are thermal conductivities in x, y and z direction, respectively.

$\{v\} = \begin{Bmatrix} v_x \\ v_y \\ v_z \end{Bmatrix}$ is the velocity vector for mass transport; $\{q\}$ is the heat flux vector, ρ is the density; c is the specific heat; T is the temperature; t is the time.

Components of thermal stress tensor were determined based on following equations:

$$\sigma_x = \frac{E_x}{h}\left(1 - (\nu_{yz})^2 \frac{E_z}{E_y}\right)(\varepsilon_x - \alpha_x \Delta T) + \frac{E_y}{h}\left(\nu_{xy} + \nu_{xz}\nu_{yz}\frac{E_z}{E_y}\right)$$

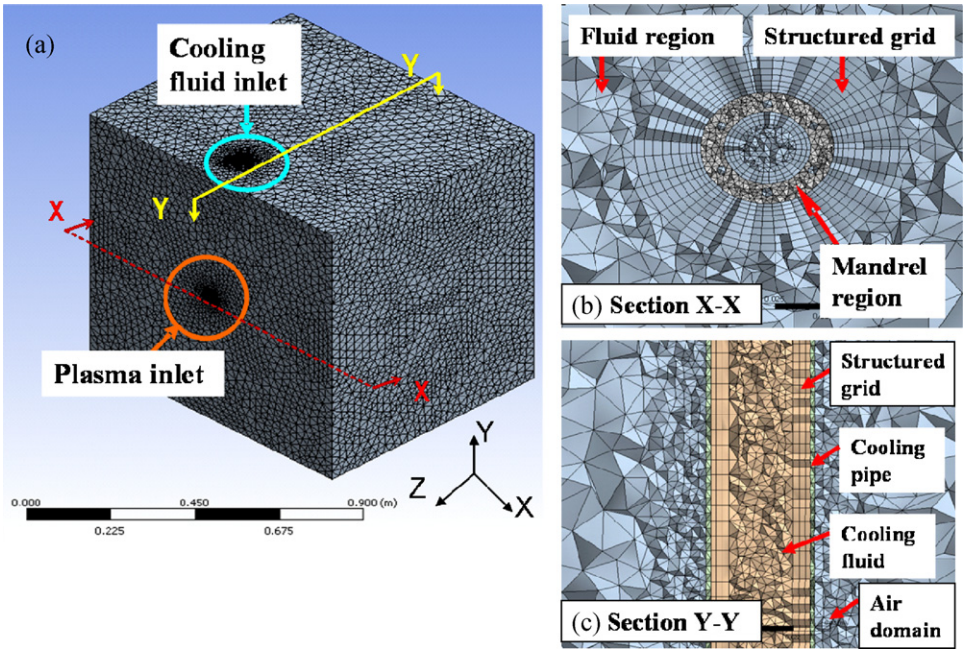

Fig. 6. (a) Grid for the entire geometry. (b) Structured grid at mandrel/air interface. (c) Grid at cooling pipe/cooling fluid interface.

Table 2
Simulation cases for three generation of the mandrels.

Mandrel generation	Simulation type	Rotating mandrel/rotating airside interface	Cooling condition	Remarks
Generation 1	Steady state	Rotating air side interface boundary	No cooling	Intense heat retention due to solid mandrel geometry resulted in coating damage. *Hence no details discussed in this paper.*
Generation 2	Steady state	Rotating air side interface boundary	No cooling	Intense heat retention due to solid mandrel geometry resulted in coating damage. *Hence no details discussed in this paper.*
Generation 3	Steady state and transient	Rotating mandrel	Air N2 CO_2 No cooling	Results are discussed for air cooling case only because it resulted in successful removal of Al_2O_3 structure from the mandrel (details are in Section 5).

$$\times(\varepsilon_y-\alpha_y\Delta T)+\frac{E_z}{h}\left(\nu_{xz}+\nu_{yz}\nu_{xy}\frac{E_z}{E_y}\right)(\varepsilon_z-\alpha_z\Delta T) \quad (2)$$

$$\sigma_y=\frac{E_y}{h}\left(\nu_{xy}+\nu_{xz}\nu_{yz}\frac{E_z}{E_y}\right)(\varepsilon_x-\alpha_x\Delta T)+\frac{E_y}{h}\left(1-(\nu_{xz})^2\frac{E_z}{E_x}\right)$$
$$\times(\varepsilon_y-\alpha_y\Delta T)+\frac{E_z}{h}\left(\nu_{yz}+\nu_{xz}\nu_{xy}\frac{E_y}{E_x}\right)(\varepsilon_z-\alpha_z\Delta T) \quad (3)$$

$$\sigma_z=\frac{E_y}{h}\left(\nu_{xz}+\nu_{yz}\nu_{xy}\right)(\varepsilon_x-\alpha_x\Delta T)+\frac{E_z}{h}\left(\nu_{yz}+\nu_{xz}\nu_{xy}\frac{E_y}{E_x}\right)$$
$$\times(\varepsilon_y-\alpha_y\Delta T)+\frac{E_z}{h}\left(1-(\nu_{xy})^2\frac{E_y}{E_x}\right)(\varepsilon_z-\alpha_z\Delta T) \quad (4)$$

$$\sigma_{xy}=G_{xy}\varepsilon_{xy},\quad \sigma_{yz}=G_{yz}\varepsilon_{yz},\quad \sigma_{xz}=G_{xz}\varepsilon_{xz} \quad (5)$$

where $h=1-(\nu_{xy})^2E_y/E_x-(\nu_{yz})^2E_z/E_y-(\nu_{xz})^2E_z/E_x-2\nu_{xy}\nu_{yz}\nu_{xz}E_z/E_x$; shear moduli $G_{xy}=G_{yz}=G_{xz}=E_x/2(1+\nu_{xy})$; stress vector $\{\sigma\}=[D]\left\{\varepsilon^{el}\right\}$, E_i is the Young's modulus in i direction, $i=x,y,z$; $[D]$ the elastic stiffness matrix, $\left\{\varepsilon^{el}\right\}$ is the elastic strain vector, ($\left\{\varepsilon^{el}\right\}=\{\varepsilon\}+\left\{\varepsilon^{th}\right\}$); $\{\varepsilon\}$ is the total strain vector $=\left[\varepsilon_x\varepsilon_y\varepsilon_z\varepsilon_{xy}\varepsilon_{yz}\varepsilon_{xz}\right]^T$; $\left\{\varepsilon^{th}\right\}$ is the thermal strain vector $=\Delta T\left[\alpha_x^{se}\,\alpha_y^{se}\,\alpha_z^{se}\,0\,0\,0\right]^T$, where α_x^{se} is secant coefficient of thermal expansion in x direction and $\Delta T=T-T_{ref}$.

4.3. Computational grid

Tetrahedral grid of 1,022,975 elements was generated for the entire plasma booth geometry including cooling fluid, cooling pipe and surrounding air region as depicted in Fig. 6(a). Inflated and structured grid with 10 layers of inflation, 1.2 expansion factor and 1 mm maximum element size was generated towards fluid

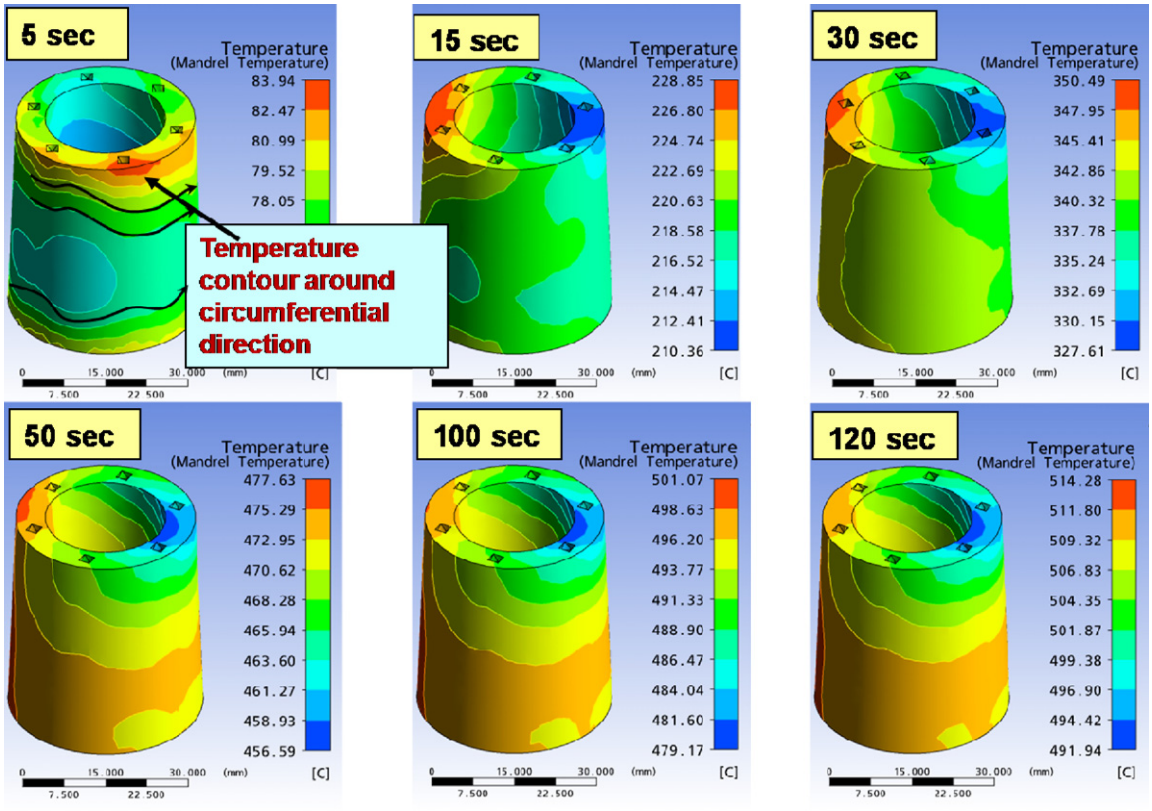

Fig. 7. Transient temperature response for generation-3 graphite mandrel at 5, 15, 30, 50, 100, 120 s.

side at the mandrel/air interface and while three layers of inflation, 1.2 expansion factor and 1 mm maximum element was generated towards fluid side at cooling media/cooling pipe interface to obtain accurate result as shown in Fig. 6 (b) and (c) correspondingly. Fine mesh with total 355,468 hex dominant elements and 1,016,436 nodes were generated for the stress analysis.

4.4. Boundary conditions

Plasma inlet velocity and plume temperature were considered as 240 m/s and 2173 °C respectively, for the computations. These values were based on the experimental results obtained using in-flight diagnostic sensor, AccuraSpray (Tecnar Automation Ltée, QC, Canada). Dust collector suction pressure was defined as 0.85 atm. It was estimated based on the loss in the duct and efficiency of the dust collector (TORIT model DFO 2-2, IG793813). Coolant inlet pressure was 1.2 bars for air cooling. A mandrel rotation speed of 120 rpm (experimental value) was considered in CFD analysis to account for the rotational effect during spraying. Transient simulation was performed up to 120 s, which is the total spraying time including preheating time, to evaluate transient temperature response of mandrel.

4.5. Computational analysis matrix

The overall matrix of the simulation work is listed in Table 2. The steady state approach was implemented to determine resultant temperature profile in generation-1 and -2 mandrels, which were assumed to be stationary. The computational model was enhanced by beta version of ANSYS CFX^{TM} 11.0 that enabled rotation of the mandrel in transient analysis for generation-3 mandrel.

5. Result and discussion

The experimental and computational work was carried out for three generations of the mandrel design and cooling conditions. Generation-1 and -2 mandrels had solid geometry and retained higher amount of heat resulting in higher temperature that caused coating cracking due to overall residual stresses. These observations were made experimentally as well as computationally. Generation-3 mandrel with a hollow geometry and internal cooling channels (Fig. 2) was found to have an optimized design where ceramic component could be formed and successfully removed with the air cooling from top at 1.2 bars. The results presented in this study focuses on the optimized design of generation-3 mandrel. Generation-1 and -2 mandrels results are not discussed here for the sake of brevity. The computational and experimental results for generation-3 mandrel are discussed below.

5.1. Computed temperature profile from the generation-3 mandrel

The transient temperature profile of the mandrel after 5, 15, 30, 50, 100 and 120 s of plasma spraying was computed and shown in Fig. 7. The effect of mandrel rotation can be clearly observed as temperature contours were spread in the circumferential direction. Also, the temperature gradient was not unidirectional. Temperature was determined in the range of 492–514 °C after 120 s. Fig. 8 shows a closer view of the temperature gradient in the mandrel/plasma and mandrel/air coolant interface. Temperature at the mandrel surface around circumferential direction was ~920 °C which reduced to 89 °C in the vicinity of mandrel/plasma interface. A similar temperature gradient was observed at the air coolant/mandrel interface where temperature reduced from 520 °C to 25 °C as shown in Fig. 8.

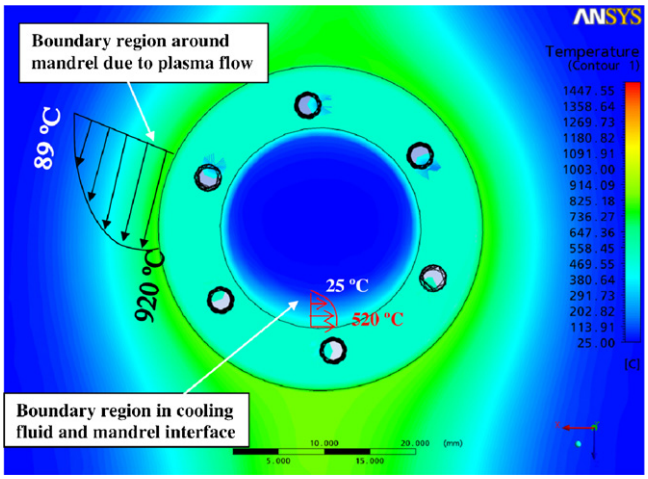

Fig. 8. A closer view of temperature profile for plasma–mandrel and cooling fluid–mandrel interaction.

5.2. Experimental validation of the temperature profile in generation-3 mandrel

Computed temperature profile in the generation-3 mandrel was compared and experimentally validated by carrying out plasma spraying of Al_2O_3 powder for ~120 s including preheating time. Mandrel was cooled with air from the top at a pressure of 1.2 bars similar to the configuration shown in Fig. 4(a). Mandrel temperature as measured by thermocouples (TC1, TC2) and infrared pyrometer (IR) during plasma spraying is shown in Fig. 9. Both thermocouples displayed almost identical temperature profile. Temperature measured by thermocouples and pyrometer showed a similar trend, though lower temperature was recorded by the pyrometer. The lower temperature displayed by the pyrometer is attributed to the varying emissivity which changes from graphite mandrel to the Al_2O_3 coating surface during plasma spraying. The peaks and valleys in the pyrometer measured temperature were due to relative motion of the plasma gun in the vertical direction and rotation of mandrel. Since pyrometer's configuration was stationary with respect to the mandrel (Fig. 4(a)), it observed hot and relatively cold surface of the mandrel resulting in localized peaks and valleys in the temperature profile. The heights of the peaks and valleys in the temperature profile measured by two thermocouples were negligible as thermocouples were not stationary with respect to the mandrel rotation. Mandrel was preheated for 15 s up to 225 °C for better splat formation (Sampath et al., 1999) and adherence of Al_2O_3 coating to the mandrel surface. The spraying of Al_2O_3 powder was carried out for 105 s with air cooling from the top that resulted in 680 μm thick coating. A maximum mandrel temperature of 594 °C was observed with the temperature increase rate (TIR) of 4.95 °C/s. The post-spraying temperature curve indicates the effect of rapid cooling due to air cooling at 1.2 bars.

The experimentally measured temperature profile (Fig. 9) was compared with the computationally predicted temperature profile (Fig. 7). Temperature of the mandrel was plotted with respect to *X* coordinate across the mandrel in the radial direction at different time intervals as depicted in Fig. 10. The experimentally measured value (shown with solid circles in Fig. 10) was mapped on the graph at the X coordinate location where thermocouples were inserted to measure temperature during spraying. Computed temperature profile (shown with solid line in Fig. 10) showed good agreement with the experimentally measured temperature profile at initial time instance. After 20 s, the computational and experimental temperature showed slight deviation of 9%. The deviation between computational and experimentally measured tempera-

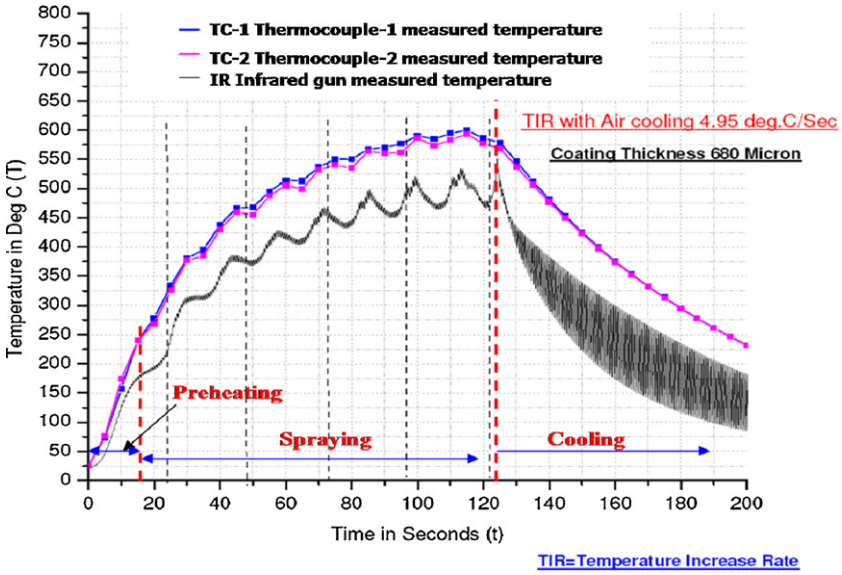

Fig. 9. Experimentally measured temperature profile for generation-3 graphite mandrel with 1.2 bars of cooling air pressure.

ture increased with increasing spray time. However, it increased to only 13% after 120 s of total spraying time. The error between computational and experimental observations is attributed to two factors: (i) computational convergence error that induced during solution of problem due to complexity of problem and (ii) loose contact between thermocouple tip and the mandrel body that caused temperature measurement error.

5.3. Computed thermal stress in ceramic coating

As computational and experimental temperature shown 87% agreement, the next step was to determine thermal stresses generated in the Al_2O_3 spray deposit and mandrel at different time intervals. The coating temperature was assumed to be same as experimentally measured value using IR pyrometer. Temperature of the mandrel was mapped from CFD results to the simulation module by one-way coupling. These transferred nodal values acted like a load to determine steady state thermal profile in both, coating and mandrel. The consolidated thermal profile of mandrel-coating assembly was applied as a thermal condition for performing stress analysis.

Thermal stress in the coating was determined at 15, 30, 60, 100 and 120 s as shown in Fig. 11. Coating thickness for the stress determination was considered as 680 μm which was an experimentally obtained value for plasma spraying duration of 120 s. Thermal stresses were found in the range of 0.16–95.3 MPa at 15 s. Thermal stress after 30 s increased to 0.27–150.6 MPa. A similar trend was observed for 60 s. However some localized high stress regions started developing in coating in axial direction as marked in Fig. 11(c). These localized stressed regions grew after 100 s and were significant at 120 s as shown in Fig. 11(e). The overall residual stress generated in coating struc-

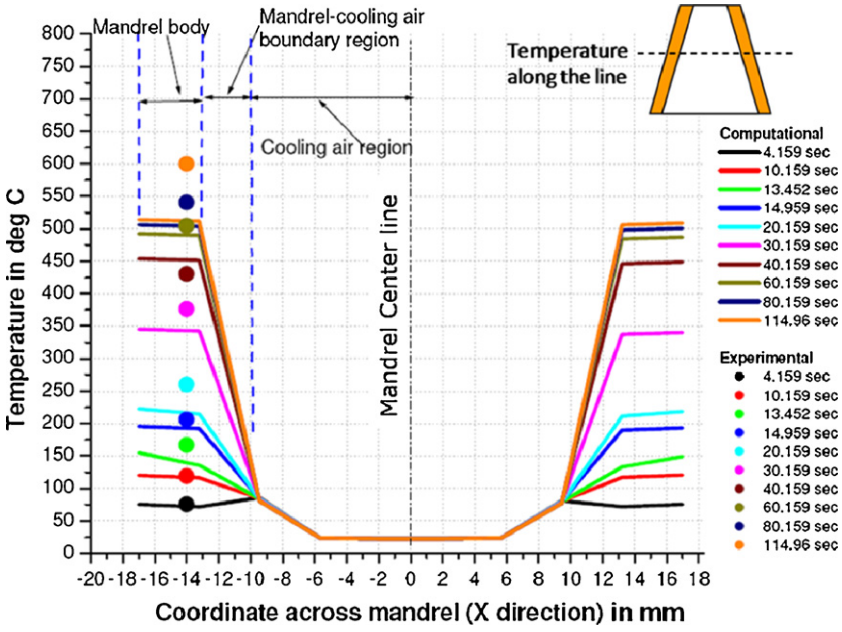

Fig. 10. Comparison of computationally predicted transient temperature (shown with solid line) variation across radial direction in mandrel with experimentally measured temperature (shown with solid circle) during plasma spraying of generation-3 graphite mandrel with air cooling.

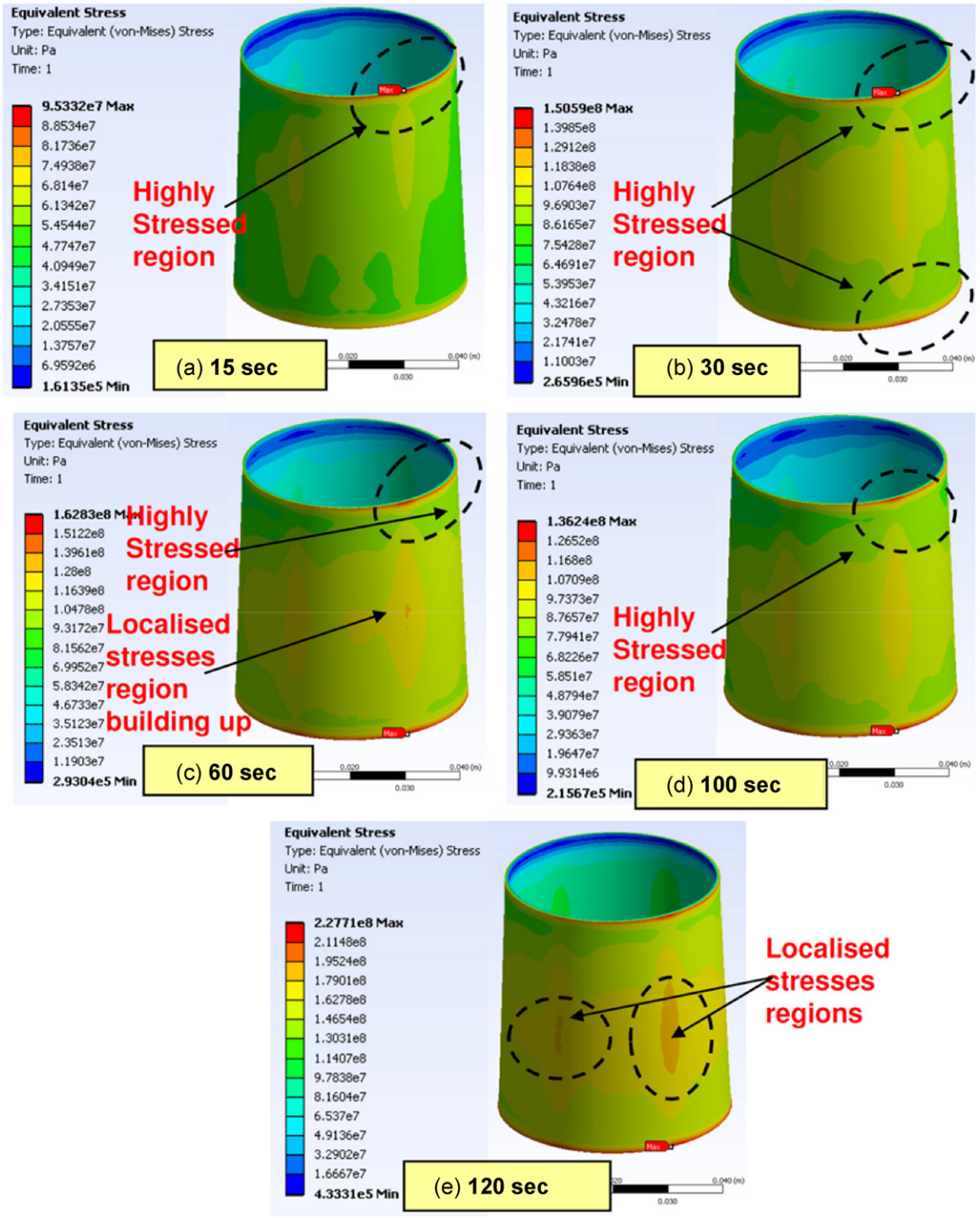

Fig. 11. Thermal stress developed at (a) 15 s, (b) 30 s, (c) 60 s, (d) 100 s and (e) 120 s, in deposition for generation-3 graphite mandrel spraying with 1.2 bars of air cooling.

ture was found to be 50.43–278 MPa (thermal stresses after 120 s to be 0.43–228 MPa + quenching stress for ceramic structure −50 MPa) which is less than the fracture strength of pure Al_2O_3, i.e. 350–450 MPa (Guimarães et al., 2009). Since overall residual stresses during deposition are lower than the fracture strength of Al_2O_3 coating, it would not crack during plasma spraying. However, it needs to be noted that spray formed Al_2O_3 coating had ~10% porosity which would lower the fracture strength of pure Al_2O_3. Hence, the fracture strength of spray formed Al_2O_3 shell with 10% porosity is expected to be higher than 278 MPa. Localized high stress region observed in Fig. 11(e) might be potential reason for formation of minor surface cracks. Subsequent to cooling the free-standing Al_2O_3 shell with a thickness of 680 μm was successfully removed from the generation-3 graphite mandrel without any damage to mandrel surface as shown in Fig. 12.

5.4. *Effect of cooling media on the mandrel temperature profile*

Based on the experimental and computational temperature profiles, a comparative analysis was done for the temperature increase rate (TIR) for the different cooling conditions for generation-3 mandrel as shown in Fig. 13. Temperature increase rate (TIR) of the

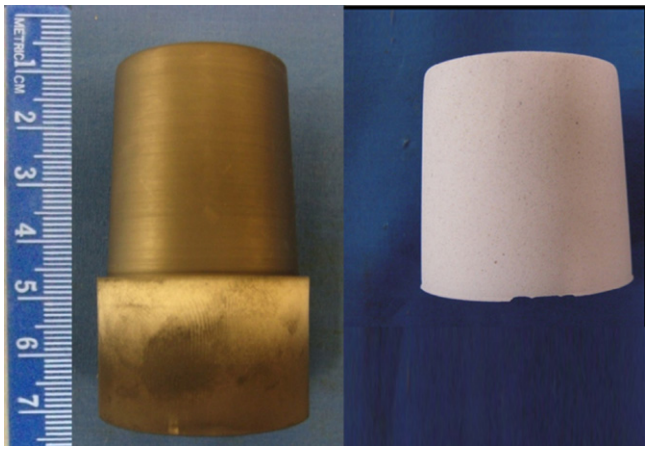

Fig. 12. Near net shape Al_2O_3 shell and generation-3 mandrel after removal of the coating.

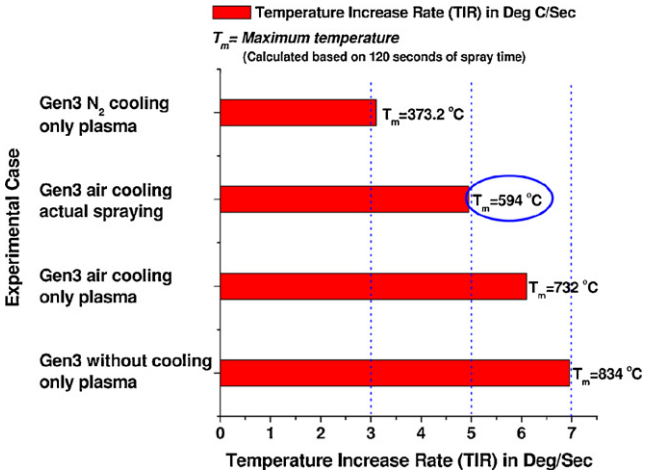

Fig. 13. Temperature increase rate (TIR) comparison for graphite mandrel with different cooling media (only plasma implies without powder whereas actual spraying means with powder feed on).

mandrel is defined as a critical parameter that governs the amount of thermal stress induced in the coating. Highest TIR (6–7 °C/s) was observed for no cooling condition whereas a lowest TIR (3°/s) was recorded for liquid N_2 cooling. A TIR of 6–7 °C/s results in an excessive temperature build up in the mandrel which causes severe stress and cracking in the coating. A low TIR value of 3 °C/s causes steep temperature gradient at the mandrel/coating interface due to high temperature of plasma and cryogenic temperature of liquid N_2 coolant. This causes thermal shock during coating deposition resulting in separation of successive splats and coating failure. An optimized TIR for generation-3 graphite mandrel with successful formation and separation of Al_2O_3 shell (Fig. 12) was found to be 4.95 °C/s where mandrel attained a maximum temperature 594 °C. Hence it can be concluded that an optimized TIR is critical for the successful deposition and removal of the thin walled ceramic near net shape. An optimized TIR results in low thermal stress and prevents crack formation in the coating. A similar combined, experimental and computational approach can be adopted for near net shape formation of other ceramic/mandrel systems by plasma spray forming technique.

6. Conclusions

A new combined experimental and computational approach has been proposed and validated for near net shape fabrication of thin walled ceramic structures by plasma spray forming (PSF) technique. Experimental temperature profile generated during spray deposition of Al_2O_3 on graphite mandrel of different geometries was successfully predicted by computational method by modeling the entire plasma booth with 87% accuracy. One-way coupling of ANSYS CFX™ and simulation module was established successfully to determine temperature profile of mandrel and corresponding thermal stresses generated in the coating. Hollow mandrel (generation 3) with air cooling from top was found the *optimum* case with successful removal of free-standing 680 μm thick Al_2O_3 structure for graphite material. Temperature increase rate (TIR) has been defined as a critical variable that determines the stress in the coating and associated cracking. An optimum TIR of 4.95 °C/s was found for Al_2O_3/graphite system which resulted in successful deposition and removal of freestanding, thin walled (680 μm) Al_2O_3 structures by plasma spray forming technique. This algorithm can be implemented to a large combination of mandrel and ceramic coating system, with minor modification in the numerical model. This protocol of predicting thermal profile of mandrel and hence thermal stresses generated in coating can be used to eliminate trial and error method to fabricate near net shape component by minimizing the number of experiments.

Acknowledgements

Financial support from the National Science Foundation CAREER Award (NSF-DMI-0547178) and Office of Naval Research (N00014-08-1-0494) is greatly acknowledged.

References

Agarwal, A., McKechnie, T., 2001. Spray forming aluminum structures. Advanced Material Process 159 (5), 44–46.
Agarwal, A., McKechnie, T., Starrett, S., Opeka, M.M., 2001. Near net shape forming of hafnium-based ceramic components: synthesis and characterization. In: Elevated Temperature Coatings-4, TMS 2001 Annual Meeting, New Orleans, USA, pp. 301–316.
Agarwal, A., Seal, S., McKechnie, T., 2002. Net shape nanostructured aluminum oxide structures fabricated by plasma spray forming. Journal of Thermal Spray Technology 12, 350–359.
Balani, K., Agarwal, A., McKechnie, T., 2006. Near net shape fabrication via vacuum plasma spray forming. Transactions of Indian Institute Metals 59 (2), 237–244.
Devasenapathi, A., Ng, H.W., Yu, S.C.M., Indra, A.B., 2002. Forming near net shape free-standing components by Plasma spraying. Materials Letters 57, 882–886.
Fang, J.C., Xu, W.J., 2002. Plasma spray forming. Journal of Materials Processing Technology 129, 288–293.
Fogarassy, P., Manescu, A., Markocsan, N., Rustichelli, F., 2004. Residual stress analysis in near net shape formed specimen obtained by thermal spraying. Physica B350, 359–537.
Gauthier, M. (Ed.), 1995. Engineered Materials Handbook Desk Edition. ASM International.
Gopalakrishnan, M.V., Metzgar, K., Rosetta, D., Krishnamurthy, R., 2003. Structural characterization and strength evaluation of spray formed ceramic composite near-net shape. Journal of Materials Processing Technology 135, 228–234.
Guimarães, F.A.T., Silva, K.G., Trombini, V., Pierri, J.J., Rodrigues, A.J., Tomasi, R., Pallone, E.M.J.A., 2009. Correlation between microstructure and mechanical properties of Al_2O_3/ZrO_2 nanocomposites. Ceramics International 35, 741–745.
Hickman, R., McKechnie, T., Agarwal, A., 2001. Net shape fabrication of high temperature materials for rocket engine components. In: Proceedings of the 37th AIAA/ASME/SAE/ASEE/Joint Propulsion Conference, Salt Lake City, UT, USA, AIAA 2001-3435.
Kuroda, S., Clyne, T.W., 1991. The quenching stress in thermally sprayed coatings. Thin Solid Films 200, 49–66.
McColm, I.J. (Ed.), 1994. Dictionary of Ceramic Science and Engineering, 2nd edition. Plenum.
Sampath, S., Jiang, X.Y., Matejicek, J., Leger, A.C., Vardelle, A., 1999. Substrate temperature effects on splat formation, microstructure development and properties of plasma sprayed coatings. Part I. Case study for partially stabilized zirconia. Materials Science and Engineering A272, 181–188.